Industrial Crops & Products 218 (2024) 119027

Contents lists available at ScienceDirect

Industrial Crops & Products

journal homepage: www.elsevier.com/locate/indcrop

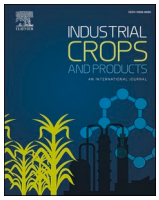

Silane-modified high-yield lignocellulosic fibers as reinforcement of polylactic acid: Enhancement of interfacial adhesion for high-performance biocomposites

Giulia Herbst [a,b], Roberto J. Aguado [a], Quim Tarrés [a], Marcos L. Corazza [b], Luiz P. Ramos [b], Pere Mutjé [a], Marc Delgado-Aguilar [a,*]

[a] LEPAMAP-PRODIS research group, University of Girona, C/ Maria Aurèlia Capmany, 61, Girona 17003, Spain
[b] Department of Chemical Engineering, Federal University of Paraná, Francisco H. Santos Av. 100, Curitiba, PR 81531-990, Brazil

ARTICLE INFO

Keywords:
Biocomposites
Polylactic acid
Interface
Silane coupling
Lignocellulosic fibers

ABSTRACT

This study investigates the enhancement of PLA-based biocomposites using high-yield mechanical stone groundwood (SGW) pulp, with a focus on reinforcing fiber-matrix interactions through silane-coupling fiber modification. Different fractions of SGW (20 and 30 wt%) and (3-glycidyloxypropyl)trimethoxysilane (GPS) as a coupling agent (3, 5, 7, and 10 wt%) were incorporated into the PLA matrix. Thermo-mechanical properties including melt flow index, melt rheology, tensile strength, and Young's modulus were evaluated, along with thermal degradation behavior via TGA and DSC. Non-modified and partially modified SGW fractions (20 and 30 wt%) improved PLA-SGW interface, resulting in increased tensile strength (14 % and 27 % respectively). Biocomposites with 30 wt% SGW modified with 5 and 7 wt% GPS exhibited the highest tensile strength improvement, along with the rest of the properties, attributed to GPS influence on melt flow index and processability. The obtained biocomposites showcased properties comparable to commodity polypropylene composites.

1. Introduction

In the last years, the need for developing sustainable and high-performance materials has been highlighted by many actors in society, including policymakers, industrial representatives, and the scientific community (Bhong et al., 2023). These materials are conceived as enablers to promote the transition from a fossil-based to a bio-based economy and, in addition, to leave behind the linear schemes to fully circular value chains (Agarwal et al., 2020; Kılıç et al., 2024; Shanmugam et al., 2021; Uppal et al., 2022). The sustainability of materials can be approached from different perspectives, including their origin, use, and end-of-life management strategies. On the one hand, the use of renewable resources for the development of value-added materials alleviates the pressure over limited resources, such as the case of petroleum (Gurunathan et al., 2015; Yatigala et al., 2018). However, 90.2 % of the global plastic production in 2021 (390.7 million tons) was fossil-based, while post-consumer recycled plastics accounted for 8.3 %, leaving a residual 1.5 % for bio-based plastics (Plastics Europe, 2022). On the other hand, the end-of-life can be approached by means of recycling strategies or through natural breakdown into simpler compounds (e.g. water, carbon dioxide, and biomass), known as biodegradation or composting, avoiding landfilling and/or incineration (Dammak et al., 2020; Sikorska et al., 2021). According to recent data in the EU27+3, the evolution of post-consumer plastics treatment exhibits a favorable scenario, having increased recycling by 117 % from 2006 to 2020. Nonetheless, landfilling stills represent around 23 %, and incineration, 42 % (Plastics Europe, 2022). In the use phase, there is an increasing need for lighter materials able to meet the technical requirements of conventional commodity materials that, for instance, can have a positive effect on the associated environmental impact of its use (Delogu et al., 2017).

Composite materials, conceptually, possess the ability to meet these requirements, providing excellent properties (e.g. mechanical, functional, lightweight) with reduced environmental impact (La Mantia and Morreale, 2011). However, the imperativeness to confront technical challenges has propelled the composite materials industry towards the development of composites reliant on fossil resources. This emphasis often prioritizes properties and production costs, yet frequently

* Corresponding author.
E-mail address: m.delgado@udg.edu (M. Delgado-Aguilar).

https://doi.org/10.1016/j.indcrop.2024.119027
Received 22 March 2024; Received in revised form 25 May 2024; Accepted 16 June 2024
Available online 20 June 2024

overlooks the adverse environmental consequences these materials entail throughout their processing, use and disposal (Rodríguez et al., 2018). Thermoplastic materials, such as polypropylene (PP), are often reinforced with short fibers to enhance their properties, achieving unconceivable levels with neat polymers (Mutjé et al., 2006). This is the case of short glass fibers (GFs), which significantly improve the mechanical performance of PP in presence of maleic anhydride functionalized PP (MAPP) as interfacial compatibilizer (Kossentini Kallel et al., 2018). While the environmental superiority of natural fiber (NF)-reinforced compared to GF-reinforced composites has been already demonstrated even 20 years ago, the latter still predominates in current market applications (Joshi et al., 2004). The environmental advantages of NF-reinforced composites are evident, encompassing the three stages highlighted above: (i) the production of NF results in lower environmental impact compared to GF, mainly due to their lower energy demands, and the amount of polymer matrix is decreased due to the demand of higher fiber content; (ii) NF are lighter than GF, resulting in lighter composites for the same application; and (iii) even if incinerated, NF-reinforced composites result in energy and carbon credits (Li et al., 2020).

In the recent years, some bio-based and biodegradable alternatives to fossil-based polymers have appeared, such is the case of poly(lactic acid) (PLA), poly(butylene adipate terephthalate) (PBAT) and poly(hydroxy alkanoates) (PHAs) (Ali et al., 2023). Considering that the end-of-life of composite materials still presents some challenges, particularly in terms of sorting and avoiding contamination of current recycling streams, the development of fully bio-based and biodegradable composites (i.e., biocomposites) is attracting the interest of both industry and scientific communities (Chatziparaskeva et al., 2022). As in the case of PP, however, ensuring appropriate interactions between fiber and polymer becomes crucial, and several efforts have been paid on the generation of well-bonded interfaces by means of incorporating coupling agents or modifying either the fibers or the polymer matrices. While it is true that fiber orientation, distribution, morphology, and dispersion have a significant impact on the resulting biocomposite mechanical properties, successfully generating these interactions ensures appropriate stress transfer between the biocomposite constituents, unlocking the reinforcing potential of the fibers (Birnin-Yauri et al., 2016; Granda et al., 2016a).

PLA is one of the most promising and most commonly used bio-based and biodegradable polymers due to its outstanding physic and mechanical properties (Madhavan Nampoothiri et al., 2010; Pang et al., 2010; Siakeng et al., 2019). Actually, PLA constitutes a competitive alternative to fossil-based polymers, exhibiting a tensile strength that can arouse between 50 and 60 MPa (Madhavan Nampoothiri et al., 2010). One strategy to further enhance its properties is the development of NF-reinforced PLA composites. However, although successfully described in the literature, uncertainty on the most appropriate surface chemical composition of the fibers still remains. In an attempt to improve interfacial fiber and biopolymer adhesion, studies on fiber surface modification mainly focus on the increase of the surface roughness by lignin removal, creating interdiffusion, and mechanical interlocking of the cellulose fraction using fiber pretreatment processes combined with dispersion agents to induce availability hydroxyl groups, capable of bonding with the polymer matrix creating a strong and stiff component (Balla et al., 2019; Lee et al., 2021). Some works have reported the suitability of partially bleached fibers to achieve a strong interfacial adhesion with PLA, while others have reported excellent results with fully bleached fibers (Delgado-Aguilar et al., 2018; Granda et al., 2016b). However, in some cases, the use of dispersants is required, and the chemical treatments for removing surface lignin inexorably generate a residual stream, questioning the overall process sustainability. Thus, the use of high-yield fibers such as mechanical or thermomechanical fibers is encouraged, as the main lignocellulosic constituents are preserved and the most significant modifications are in terms of morphology (Mujtaba et al., 2023). Concretely, the direct fibrillation of wood fibers generates a significant increase on surface roughness, together with fine elements with high surface area that can improve the fiber reinforcing potential (Graupner et al., 2023). Other strategies encompass the implementation of silane-coupling between fibers and polymers, enhancing fiber hydrophobicity and promoting their dispersion and interactions with PLA (Chen et al., 2021). The surface silanization of the main lignocellulosic fraction, cellulose, promotes the generation of hydrogen bonds between hydroxyl groups and silane coupling agent, creating a " bridge-like " effect that improves the composite's interfacial compatibility and mechanical properties (Tian et al., 2023, 2022). In previous works, silane coupling agents were efficiently condensed to the fiber surface through reactions involving hydroxyl and alkoxy groups capable of grafting both fiber and polymer (Chen et al., 2021; Luo et al., 2016; Yang et al., 2023a). Also, the presence of lignin increases the availability of hydroxyl groups that can couple with reactive silanol groups. Studies by Zhu et al. (2015), Yeo et al. (2017), and Wang et al. (2020) demonstrated an increase in tensile strength and improvement in the miscibility of silane-treated lignin composites with unsaturated polyester resins and PLA. Previous research has suggested using (3-glycidyloxypropyl)trimethoxysilane as a coupling agent to fiber silanization. The presence of three methoxy groups increases its availability for undergoing hydrolysis and condensation into the fiber. Additionally, the terminal epoxy group can enhance compatibility with the PLA matrix, facilitating the development of a monolayer or a three-dimensional covalent network on the fiber chains (de Buyl and Kretschmer, 2008; Yang et al., 2023b).

For all the above, the present work aims at elucidating the suitability of incorporating stone groundwood fibers (SGW) from pine into PLA at different fiber contents, together with the influence of GPS as coupling agent. A comprehensive assessment of the biocomposite properties is provided, as well as a strategy for developing fully bio-based and biodegradable biocomposites using high-yield fibers, constituting a strong alternative to commodity composites (e.g. PP/GF) for several of applications.

2. Experimental

2.1. Materials

PLA with 1.24 g/cm^3 density (Ingeo Biopolymer 4043D) was supplied by Natureworks (Minneapolis, MN, USA) and used as biodegradable thermoplastic matrix. A commercial grade of stone groundwood pine pulp (SGW) was kindly provided by Zubialde S.A. (Aizarnazabal, Spain). The pulp was supplied in the form of dried blocks, with a moisture content below 10 % by weight. Fibers were modified by the incorporation of modified amounts of (3-glycidyloxypropyl)trimethoxysilane (GPS), also known as silane coupling agent KH560, acquired at Merck (Barcelona, Spain).

2.2. Fiber preparation and characterization

SGW was dispersed in water using a baffled pilot scale pulper at a consistency of 5 wt% at room temperature and 1100 rpm for 30 min. The selected rotor configuration was centered and helicoidal. This dispersion process enabled the disintegration of the starting blocks, leading to fiber individualization and pulp dispersion in water. The pulper was then discharged and further diluted with water until reaching a pulp consistency of 3 wt% under mechanical stirring.

The SGW silanization process was performed by the dropwise addition of GPS at different GPS-to-fiber ratios, ranging from 0 % to 10 %, into the SGW pulp dispersed in water (pulp consistency of 3 wt%) under gentle stirring for 30 min. The fibers were then filtered over a 200-mesh nylon cloth and air-dried for 48 h. The samples were labeled according to the GPS content (e.g., the sample containing 5 % of GPS was labeled as SGW5).

The characterization of the fibers included morphological analysis

using MorFi equipment equipped with a CCD video camera able to analyze 30,000 fibers per batch. The equipment is controlled by the MorFi v9.2 software and provides the main morphological features of the fibers, including average fiber diameter and length, fines content (fibers shorter than 75 μm), and size distribution. The morphology of composite extracted fibers was also measured. PLA30SGW and PLA30SGW5 samples, around 5 g, were solubilized in 50 mL chloroform-DMF (dimethyl formamide) 4:1 v/v solution under agitation during 24 h. The extracted fibers were filtered using a vacuum pump, washed with acetone, and further washed with distilled water. The morphological analysis was performed after oven-drying at 105 °C for 24 h.

Fiber chemical composition was determined according to TAPPI standards. SGW was prepared for chemical characterization according to TAPPI standard T257, drying them in an oven at 105 °C until constant weight. The dried SGW was then milled and sieved (40 mesh). Extractives were determined in a Soxhlet apparatus using an ethanol-toluene mixture as solvent (TAPPI T204). A blank determination was also carried out with the solvent used in the test. The solvent-free sample was then used for lignin determination according to TAPPI standard T222, quantifying acid-insoluble lignin. Finally, cellulose content was determined by high-performance anion exchange chromatography (HPAEC), as reported by Tarrés et al (Granda et al., 2016a), and hemicellulose was estimated by subtracting from 100 %.

FTIR-ATR spectroscopy analysis was performed to assess the effect of the coupling agent on the treated and untreated SGW chemical composition using a compact spectrometer Alpha II (Bruker Corporation, Massachusetts, United States). Spectra were acquired from a platinum ATR accessory at a resolution of 4 cm^{-1} within the 400–4000 cm^{-1} wavenumber range.

2.3. Compounding of fiber-reinforced biocomposites

Previously dried SGW samples, both GPS-modified and not, were incorporated at 20 and 30 wt% into the PLA matrix using a high-speed kinetic mixer (Gelimat, Draiswerke Inc, NJ, USA). The SGW fibers were first incorporated into the mixing chamber at a low rotational speed (315 rpm) and then, PLA was also incorporated. The rotational speed was gradually increased up to 3000 rpm, reaching a temperature of 195 °C, enabling the melting of the polymeric matrix and fiber wetting and dispersion. Each biocomposite formulation was discharged, separated into small pieces, and milled using a knife mill (SM 100, Retsch GmbH, Haan, Germany) equipped with a 4 mm sieve at the bottom. The samples were stored in an oven at 80 °C to avoid moisture absorption. PLA20SGW and PLA30SGW (0, 3, 5, 7, and 10 % of GPS) standard specimens for tensile test were obtained by injection molding, using a plastic injection molding machine Allrounder (model 320 C 500–170, series 205029, Arburg GmbH + Co KG, Lossburg, Germany) according to ASTM D638 standard.

2.4. Characterization of the biocomposites

2.4.1. Melt flow index (MFI)

Melt Flow Index (MFI) was determined in a CEAST testing equipment (7082,000, series 17959, Pianezza, Italy), according to ISO 1133 standard. The extrusion rate was determined as the mass extruded over a specified time at 210 °C and a load of 2.16 kg, as suggested by the PLA supplier. Approximately 6 g of each material was placed into the die, and the MFI was expressed in g/10 min, representing the amount of material that flows through the equipment in 10 min

2.4.2. Density

The density of the biocomposites was determined using the liquid pycnometer method, as specified in the ISO 1183–1 standard. To perform the analysis, approximately 3 g of ground tensile specimens were added to a 50 cm^3 glass pycnometer and filled with distilled water at room temperature (21 °C) as immersion liquid.

2.4.3. Melt rheology

The rheology measurements were conducted according to the ASTM D4440–15 standard on a modular rheometer (model MCR 302e, Anton Paar GmbH, Graz, Austria) in oscillatory mode. A parallel plates geometry arrangement with a gap of 1 mm was employed, and the measurements were taken in the PLA melt state at 190 °C. The frequency range used was set between 0.1 and 100 Hz. The linear viscoelastic region was determined using an amplitude sweep deformation of 5 %, with controlled shear deformation. The storage and loss modulus, and the complex viscosity of the composites were measured by the TruStrain™ software.

2.4.4. Mechanical properties

Neat PLA and PLA/SGW biocomposite specimens were conditioned on a climatic chamber (Dycometal, Barcelona, Spain) according to ISO D618 standard for 48 h at 23 °C and 50 % relative humidity and tested on a universal testing machine (DTC-10, IDM Test S.L, San Sebastian, Spain). The tensile strength was performed according to ASTM D638 standard at 2 mm/min and equipped with a 5 kN load cell. For Young's modulus determination, an extensometer was coupled to the specimens. The test was performed until 0.25 % strain on the stress-strain plot according to the ASTM D638 standard. Mechanical properties were expressed as the average of 5 tested specimens of each sample.

2.4.5. Electron microscopy

The surface of the fractured tensile samples was analyzed by field emission scanning electron microscopy (FE-SEM, Hitachi S-4100, Japan). The samples were previously fixed on a sample holder using a conductive carbon tape and coated with a carbon layer using a turbo evaporator device (Emitech K950, Germany) to avoid surface charging during the analysis. Images were taken using the Quartz PCI software at accelerating voltages of 5.0 kV and magnification of 600x, with a secondary electron detector (SED).

2.4.6. Thermal analysis

Thermogravimetric analysis (TGA) was performed to assess the effect of incorporating the SGW fibers on the thermal stability of the PLA matrix, using a thermogravimetric analyzer (Mettler-Toledo, LLC, USA). Analyses were performed from 30 to 600 °C at a heating rate of 10 °C min^{-1} under an inert nitrogen atmosphere. The thermal behaviors of neat PLA and PLA/SGW biocomposites were analyzed by differential scanning calorimetry (DSC) to evaluate the physical properties related to the material transition measurement (DSC822e, Mettler-Toledo, LLC, USA). Samples were analyzed at a heating/cooling rate of 10 °C min^{-1} from 30 to 210 °C under an inert N_2 atmosphere. The degree of crystallinity, *Xc (%)*, was calculated with the first heating scans (given that the thermal history involved curing) as a function of melt and cold-crystallization enthalpies (ΔH_m and ΔH_{CC}, respectively), and the PLA theoretical melting enthalpy (ΔH°_m):

$$X_c = (100\ x\ (\Delta H_m - \Delta H_{CC}))/\ (\Delta H^\circ_m\ x\ PLA_{fraction}) \quad (1)$$

considering ΔH°_m as 93.6 J/g for 100 % crystalline PLA (Hakim et al., 2017).

2.5. Micromechanical modelling

The micromechanics of the developed biocomposites was approached by combining the modified rule of mixtures (mRoM), the Hirsch model, and the Tresca and Von Misses criteria for the interfacial shear stress (IFSS) calculation, together with the determination of the critical length (L_c^F). The input data consisted of both stress-strain curves and average data from the matrix and biocomposite tensile tests, as well as the morphological features (average length, diameter, and fines content in length) of the extracted fibers.

The matrix contribution to the biocomposite tensile strength (σ_t^{m*})

Table 1
Chemical composition and morphological features of SGW.

Chemical composition				Fiber morphology		
Cel (%)	HCel (%)	KL lignin (%)	Ext (%)	L^F (μm)	d^F (μm)	f (μm)
42.3 ± 1.6	27.1 ± 2.1	29.6 ± 1.8	1.9 ± 0.2	497 ± 31	25.9 ± 1.8	40.5 ± 2.5

was determined by calculating the tensile strength of the matrix at the elongation at the break of each biocomposite, previously fitting the stress-strain curve of the PLA matrix to a fifth-order polynomial equation (Eq. 2). Then, the mRoM was used to determine the value of the fiber tensile strength factor (Eq. 3, where V^F stands for the volume fraction of the fiber within the biocomposite), resulting from the product between the coupling factor (fc) and the intrinsic tensile strength of the SGW fibers (σ_t^F) according to Eq. 4.

$$\sigma_t^{PLA} = -0.0574\varepsilon_t^5 - 0.6947\varepsilon_t^4 + 5.7427\varepsilon_t^3 - 13.6\varepsilon_t^2 + 29.836\varepsilon_t + 0.8673 \quad (2)$$

$$\sigma_t^c = FTSF \cdot V^F + \left(1 - V^F\right)\sigma_t^{m*} \quad (3)$$

$$FTSF = f_c \cdot \sigma_t^F \quad (4)$$

In parallel, the intrinsic tensile modulus of the fiber (E_t^F) was calculated using the Hirsch model (Eq. 5).

$$E_t^c = \beta\left[E_t^F \cdot V^F + E_t^m\left(1 - V^F\right)\right] + (1-\beta)\frac{E_t^F \cdot E_t^m}{E_t^m \cdot V^F + E_t^F\left(1 - V^F\right)} \quad (5)$$

where E_t^c and E_t^m are the elastic modulus of the biocomposite and the matrix, respectively, both obtained during the tensile test, and β is the stress transfer factor (Serra-Parareda et al., 2021). A value of 0.4 was assigned to this factor, as previously reported. The average E_t^F was then calculated and, considering an elastic behavior of the developed biocomposites, the average σ_t^F was obtained.

The IFSS was estimated through the Tresca and Von Misses criteria, τ_T and τ_{VM}, according to Eqs. 6 and 7, respectively.

$$\tau_T = \frac{\sigma_t^c}{2} \quad (6)$$

$$\tau_{VM} = \frac{\sigma_t^c}{\sqrt{3}} \quad (7)$$

Critical length (L_c^F) was calculated according to Eq. 8, considering that most of the biocomposite fibers corresponded to subcritical fibers. The interface factor (χ_2) and the fiber orientation factor (χ_1) were calculated according to Eqs. 9 and 10:

$$L_c^F = \frac{\sigma_t^F \cdot d^F}{2 \cdot \tau} \quad (8)$$

$$\chi_2 = \frac{\tau \cdot L^F}{\sigma_t^F \cdot d^F} \quad (9)$$

$$f_c = \chi_1 \cdot \chi_2 \quad (10)$$

where d^F and L^F correspond to the fiber diameter and length, both expressed in μm, respectively.

3. Results and discussion

3.1. Characterization of the fibers

The chemical composition and the main morphological features of the SGW pulp are shown in Table 1. This includes the cellulose (Cel), hemicellulose (HCel), Klason lignin (KL lignin), and extractives (Ext) contents in what pertains to the chemical composition, and the fiber length weighted in length (L^F), average fiber diameter (d^F), and fines content (f) regarding morphology.

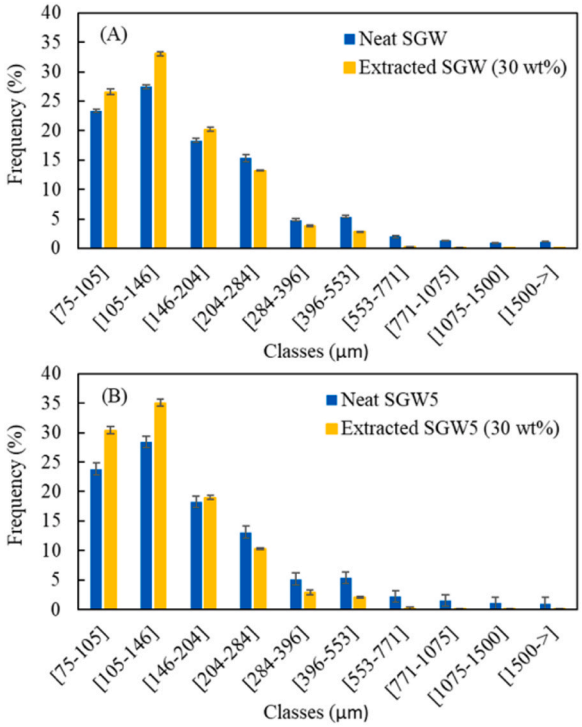

Fig. 1. Fiber length distribution before and after injection of untreated SGW (A) and SGW5 (B).

SGW pulp exhibited a chemical composition similar to that of pine wood, containing 42–52 % cellulose, 24 – 28 % hemicelluloses, 22 – 28 % lignin, and 2 – 3 % extractives (Ferraz et al., 2000; Maaoui et al., 2023; Reyes et al., 2013; Sable et al., 2012). These similarities are expectable, considering that SGW is a mechanical pulp produced by mechanical fibrillation using cold water as lubricant, which results in high production yields, slight chemical modifications and minimized side-stream generation (López et al., 2012). Chemical composition imparts remarkable effects on fiber dispersion and their interaction with the polymer matrix (Yang et al., 2019). However, the chemical interface between PLA and natural fibers has not been successfully addressed in the literature. Apparently, the hydrophobic character of PLA should hinder its interactions with hydrophilic natural fibers. Previous studies revealed that the presence of lignin could benefit these interactions, mainly due to its hydrophobic character. Exemplarily, the presence of moderate amounts of lignin in jute fibers enhanced their interfacial adhesion with PLA, boosting tensile strength by 46 % with a 30 wt% addition of partially bleached jute fibers (Delgado-Aguilar et al., 2018). However, the role of lignin in the absence of any coupling agent can be attributed to achieving a better fiber dispersion within the polymer matrix, rather than generating strong interfaces. In a previous study, the surface properties of SGW and bleached kraft pine pulp were used to demonstrate that cellulose has a higher affinity for PLA than lignin (Granda et al., 2016a). In this sense, and aligned with previous works on PLA/lignin composites, the use of GPS should benefit from the improved dispersion provided by lignin, enhancing interface properties by silanization of the fiber surface (Tan et al., 2023; Wang et al., 2020; Zhu et al., 2015).

In addition to chemical composition, fiber morphology also has a pivotal role in the reinforcing potential of fiber-reinforced composites, particularly the length-to-diameter ratio, known as the aspect or slenderness ratio. As revealed in Table 1, SGW exhibited a fiber length and

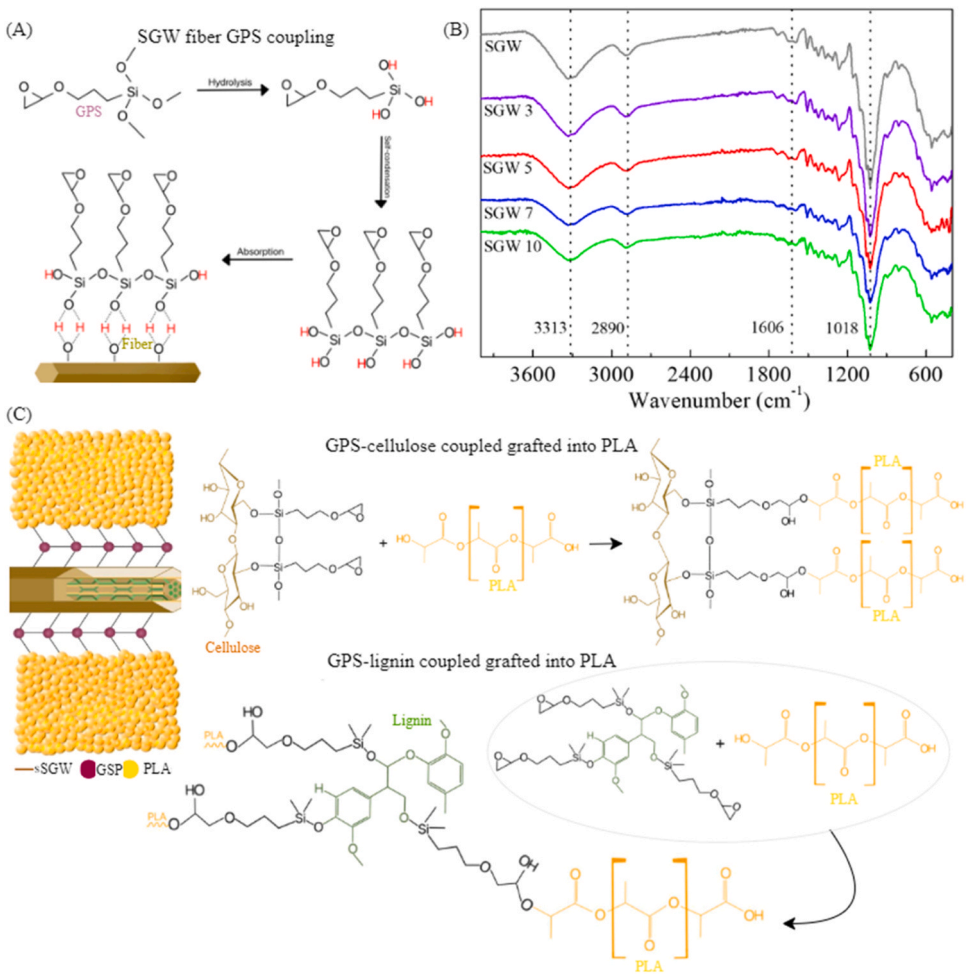

Fig. 2. (A) Fiber coupling agent silanization reaction; (B) FT-IR spectra of untreated and GPS-treated SGW at different concentrations; (C) Fiber-GPS-PLA bonding scheme, possible mechanism for cellulose and lignin.

diameter of 497 and 25.9 μm, respectively, leading to an aspect ratio of 19.2. However, during compounding and injection molding, fibers experience shortening due to the shear stress among fibers, with the polymer matrix, and with the cavity of the processing equipment (Wang et al., 2011). This generates a disentanglement of the fiber bundles, exposing more surfaces to be wetted by the matrix and increasing the susceptibility to fiber-matrix interactions (Hasan et al., 2022). Fig. 1 provides the fiber length distribution of the unmodified SGW before and after compounding (extracted from the biocomposites at 30 wt% fiber content), as well as of the SGW5 for comparison.

Fig. 1 reveals that, as mentioned above, the injection molding generates a significant fiber shortening, shifting the length distribution to the left. In comparative terms, the average fiber length of the untreated SGW decreased from 497 to 205 μm, representing a shortening of 59 %. However, fiber diameter did not experience significant changes. In the case of the SGW5, fiber shortening was of the same magnitude, starting at 493 μm and ending at 192 μm after the injection process, while in the case of the untreated SGW, fiber diameter remained constant. However, in both cases, a significant increase in the fine content was observed, starting at 43 % approximately for both fibers and ending at around 60 %. This high increase indicates that the compounding and the injection process highly fibrillates the fibers and that some of the fiber particles are not considered in the fiber length distribution from Fig. 1. In addition, fine fibers are expected to exhibit lower diameters. Hence, the MorFi equipment could not detect the effect of these high surface area fibrils on the evolution of biocomposite strength.

The chemical composition and morphology of lignocellulosic fibers play a pivotal role in composite formulation, directly related to the performance of its thermomechanical properties (Granda et al., 2016a). However, to enhance the compatibility between the PLA polymer matrix, formed by weakly polar ester bonds, and the hydroxyl groups of the lignocellulose structure, the SGW pulp required partial surface modification. As previously discussed, Granda et al. (2016b) explored the use of diethylene glycol dimethyl ether as a dispersant agent for bleached kraft softwood fibers, with the purpose of avoiding fiber agglomeration during compounding. In further studies, Delgado-Aguilar et al. (2018) observed that the mechanical performance of PLA/jute fiber composites increased in the presence of an optimum lignin content after fiber bleaching.

However, from a resource-efficiency perspective, the preservation of the lignocellulosic constituents should be set as a priority. Lignin concentration is higher at the outer layers of the lignocellulosic fibers and most of the interactions with PLA, in case of using high-lignin fibers as reinforcement, would take place with lignin rather than with cellulose. Studies by Chen et al. (2021), Wang et al. (2020), and Zhu et al. (2015) investigated the application of silane coupling agents for constructing compatible interfaces between PLA/fiber and PLA/lignin and improving its thermo-mechanical properties, since silane reactive groups bind to the carboxyl-terminal groups of PLA and to the lignocellulose hydroxyl groups, as represented in Fig. 2 (A), resulting in improvements around 40 and 43 % for bending and tensile strengths, respectively.

Modifications on the SGW chemical structure after 3, 5, 7, and 10 wt % GPS treatment were assessed by FT-IR spectroscopy (Fig. 2B). The main representative bands related to cellulose, hemicelluloses, and

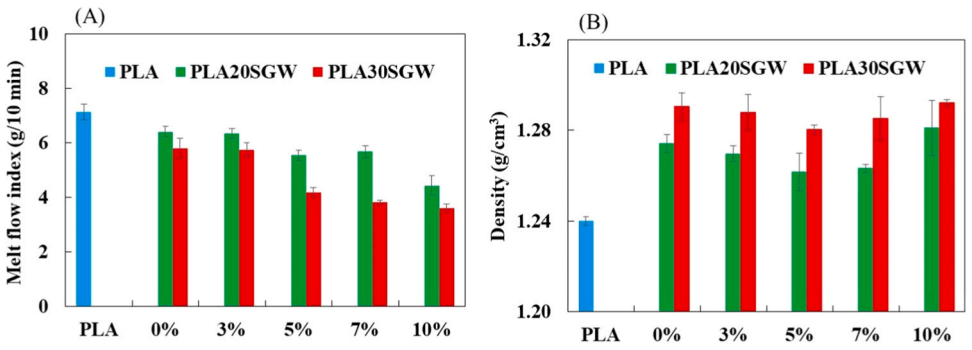

Fig. 3. Evolution of Melt Flow Index (A) and density (B) with the incorporation of GPS for the different levels of SGW reinforcement (20 and 30 wt%).

lignin were centered at 3313 cm^{-1} for the O−H intra- and intermolecular stretching hydroxyl groups, at 2890 cm^{-1} for the C−H stretching methyl and methylene groups, at 1606 cm^{-1} for aromatic ring vibration attributed to lignin, and at 1018 cm^{-1} for the C–O–C asymmetric stretching in carbohydrates and the C–H in-plane deformation in aromatic groups (Javier-Astete et al., 2021; Méndez et al., 2007).

By increasing the GPS concentration from 0 to 10 wt%, a proportional reduction in the O–H stretching vibrations was noticed, demonstrating that part of the available lignocellulose hydroxyl groups were grafted by silanol groups formed after Si−OCH_3 hydrolysis of the coupling agent in aqueous media (Chen et al., 2021). However, there was no clear evidence for fiber silanization, since sharp Si–O–C vibrations at 1000–1200 cm^{-1} and Si−O−Si vibrations (from silanol self-polymerization) at 700–800 cm^{-1} were not present in the spectra (Barczewski et al., 2020; Chen et al., 2021; Liu et al., 2019; Zhang et al., 2022).

The fiber silanization and grafting mechanism, for both lignin and cellulose into PLA structure, is represented in Fig. 2C. It comprehends the coupling agent (GPS) hydrolysis, from silane into silanol groups, and the possible self-condensation between the silanol hydroxyl groups, due to its high reactivity. Then, the formation of hydrogen bonds with the fiber surface leads to subsequent adsorption and grafting, characterized by the formation of covalent bonds (during the fiber drying process) between the silanols and the hydroxyl groups of the fibers (Arslan and Dogan, 2018; del Angel-Monroy et al., 2024; Qian et al., 2023).

3.2. *Physical and mechanical properties of biocomposites*

Changes in MFI and density provided useful insights of the effects of SGW incorporation into the polymer matrices, both in terms of

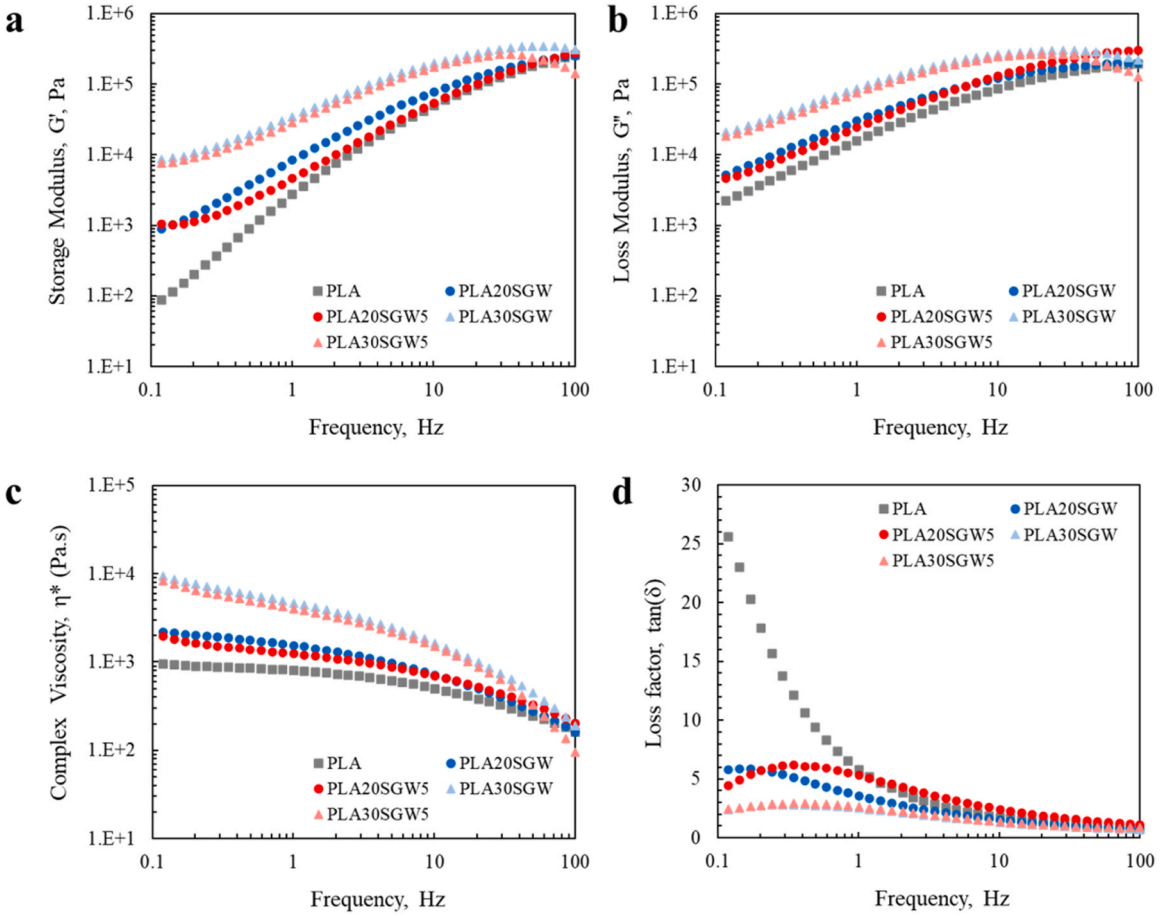

Fig. 4. Rheological features of the neat PLA and the PLA composites containing unmodified and 5 wt% GPS-modified SGW (20 and 30 wt%).

Table 2
Tensile properties of the PLA/SGW biocomposites.

SGW (wt %)	V^f	GPS (wt %)	σ_t^c (MPa)	E_t^c (GPa)	ε_t^c (%)	σ_t^{m*} (MPa)
0	0.0	0	53.27 ± 2.14	3.8 ± 0.1	3.22 ± 0.01	-
20	0.151	0	60.94 ± 1.79	5.2 ± 0.1	3.12 ± 0.09	53.18
		3	62.25 ± 1.38	5.7 ± 0.2	2.80 ± 0.19	51.27
		5	66.15 ± 0.62	5.2 ± 0.1	2.93 ± 0.11	52.39
		7	64.86 ± 0.79	5.3 ± 0.1	2.88 ± 0.09	52.01
		10	64.58 ± 1.19	5.5 ± 0.1	2.87 ± 0.07	51.92
30	0.229	0	67.77 ± 0.65	6.8 ± 0.1	2.62 ± 0.08	49.14
		3	68.36 ± 1.62	7.1 ± 0.3	2.76 ± 0.12	50.85
		5	73.19 ± 2.08	6.8 ± 0.2	2.84 ± 0.28	51.66
		7	74.21 ± 0.79	6.6 ± 0.1	2.78 ± 0.05	51.06
		10	68.89 ± 2.30	6.5 ± 0.1	2.69 ± 0.16	50.04

σ_t^c: tensile strength; E_t^c: Young's modulus; ε_t^c: elongation at break; σ_t^{m*}: contribution of the matrix to tensile strength

processability and specific weight of the resulting biocomposites. Fig. 3 shows the evolution of both MFI and density at different SGW fiber contents (20 and 30 wt%) and GPS modification degrees.

Natural fiber-reinforced composites exhibit shear-thinning behavior that contributes to the decrease of MFI values as fiber content is increased (Fig. 3A) (Awal et al., 2015). The MFI of the PLA matrix decreased from 7 g/10 min to nearly 6 g/10 min at 30 wt% fiber content and finding its minimum with 30 wt% of SGW and between 7 % and 10 % GPS. Hence, fiber incorporation in the PLA matrix decreases the composite MFI; consequently, the fibers do not melt and contribute to the viscosity of the polymer due to fiber-polymer interactions, leading to higher melt strength than the neat polymer (Awal et al., 2015; Long et al., 2019). Furthermore, as discussed above, SGW is a highly fibrillated pulp, counting on a pronounced surface fibrillation due to the processing conditions. This highly fibrillated surface, together with the generation of shorter and finer fibers during compounding, significantly contribute to the fiber interactions with the polymer and, thus, to its flowability (Bianchi et al., 2019; Hietala et al., 2014; Jalaee and Foster, 2024).

Considering that fiber-polymer interactions also affect chain mobility in the melt state, concretely, for a certain fiber content, increasing GPS resulted in lower MFI, indicating that the presence of GPS promoted the adhesion of the two biocomposite phases (Luo et al., 2016). Fan et al. (2023) also reported a linear decrease in MFI values as the fiber and the coupling agent contents were increased. Actually, some authors reported that the melt rheology of fiber-reinforced composites provide useful information about fiber-matrix interactions (El Omari et al., 2023; Fourati et al., 2021; Hristov and Vlachopoulos, 2007). Fig. 4 shows the storage modulus (G'), loss modulus (G''), complex viscosity (η*), and the loss factor (tan (δ)) of different biocomposites compared to PLA.

Fig. 4 reveals significant differences at low shear rates with the incorporation of SGW, particularly in terms of G', G'' and η*. At low shear rates, G'' dominated over the G', clearly suggesting that materials exhibited predominantly a viscous behavior. However, these differences became lower as the fiber content was increased, as illustrated by Fig. 4D, where the loss factor is provided. At low shear rates, the viscous behavior of PLA was much more accentuated than in the case of the resulting biocomposites, which exhibited lower loss factor values. This effect, provided by the inclusion of fibers into the PLA matrix, is

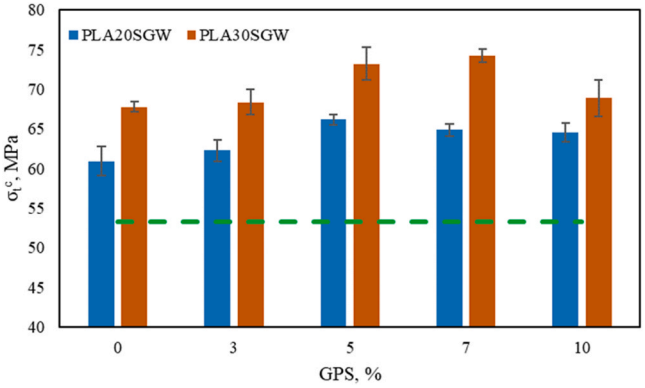

Fig. 5. Evolution of σ_t^c of PLA biocomposites at different GPS and SGW contents. The green dashed line corresponds to the neat PLA.

attributed to the presence of a strong network of fibers within the polymer matrix (Safdari et al., 2018). In addition, at low frequencies, the obtained G' for the biocomposites containing 30 wt% SGW were found to be up to two orders of magnitude higher, confirming these interactions. As the amount of fiber was increased in the biocomposites, the loss factor became lower, indicating its predominantly elastic behavior. In addition, regardless the fiber content, a crossover point was normally found between 40 and 50 Hz. While the presence of GPS had a direct influence on MFI and, as later discussed, in the mechanical properties of the obtained biocomposites, no significant effects were found over its rheological behavior in the melt state, as previously observed for PLA biocomposites reinforced with silane-coupled lignocellulosic fibers (Chen et al., 2021).

Table 2 provides the tensile strength characteristics of the obtained biocomposites as function of fiber and GPS contents. In all cases, regardless the GPS content, the tensile strength and Young's modulus were increased. The incorporation of neat SGW enhanced the tensile strength of the composite by 14.4 and 27.2 % for an addition of 20 and 30 wt%, respectively. For the same fiber content, the incorporation of 5 % GPS enhanced these properties by 24.2 and 37.4 %. In addition, the presence of GPS gradually increased the reinforcing capacity of SGW, reaching a plateau between 5 % and 7 % to be decreased afterward with a 10 % addition. This effect was not observed in the Young's modulus, where a significant enhancement was obtained regardless the GPS content.

Tensile strength measurements revealed the potential of PLA biocomposites to replace several commodity PP composites reinforced, for instance, with glass fiber. The incorporation of 20 wt% glass fiber into PP generates materials with a tensile strength of around 60 MPa and densities of 1.35 g/cm^3 (Eftekhari and Fatemi, 2016). These tensile strengths were already achieved with 20 wt% SGW in PLA with densities below 1.28 g/cm^3, representing a competitive advantage for obtaining lighter materials with similar mechanical properties that, in turn, come from bio-based resources and can be biodegraded at their end of life. Moreover, SGW processing is safe and well-stablished, while glass fiber handling imparts negative effects on the environment and on human health, particularly for workers directly involved in the process (Gonçalves et al., 2022).

The incorporation of silane coupling agent evidenced a reduced fiber debonding from the matrix under stress. Fig. 5 reveals that the maximum performance of the biocomposites was reached between 5 % and 7 % of GPS with respect to SGW content.

The mechanism of silane coupling in lignocellulosic fiber biocomposites has been previously reported, revealing that layers of coupling agents are formed during GPS grafting and/or adsorption onto the fiber surface as covalent and hydrogen bonds, and the epoxy organofunctional group leads to interdiffusion with the polymeric matrix (Arslan and Dogan, 2018). This contributes to successful reinforcement

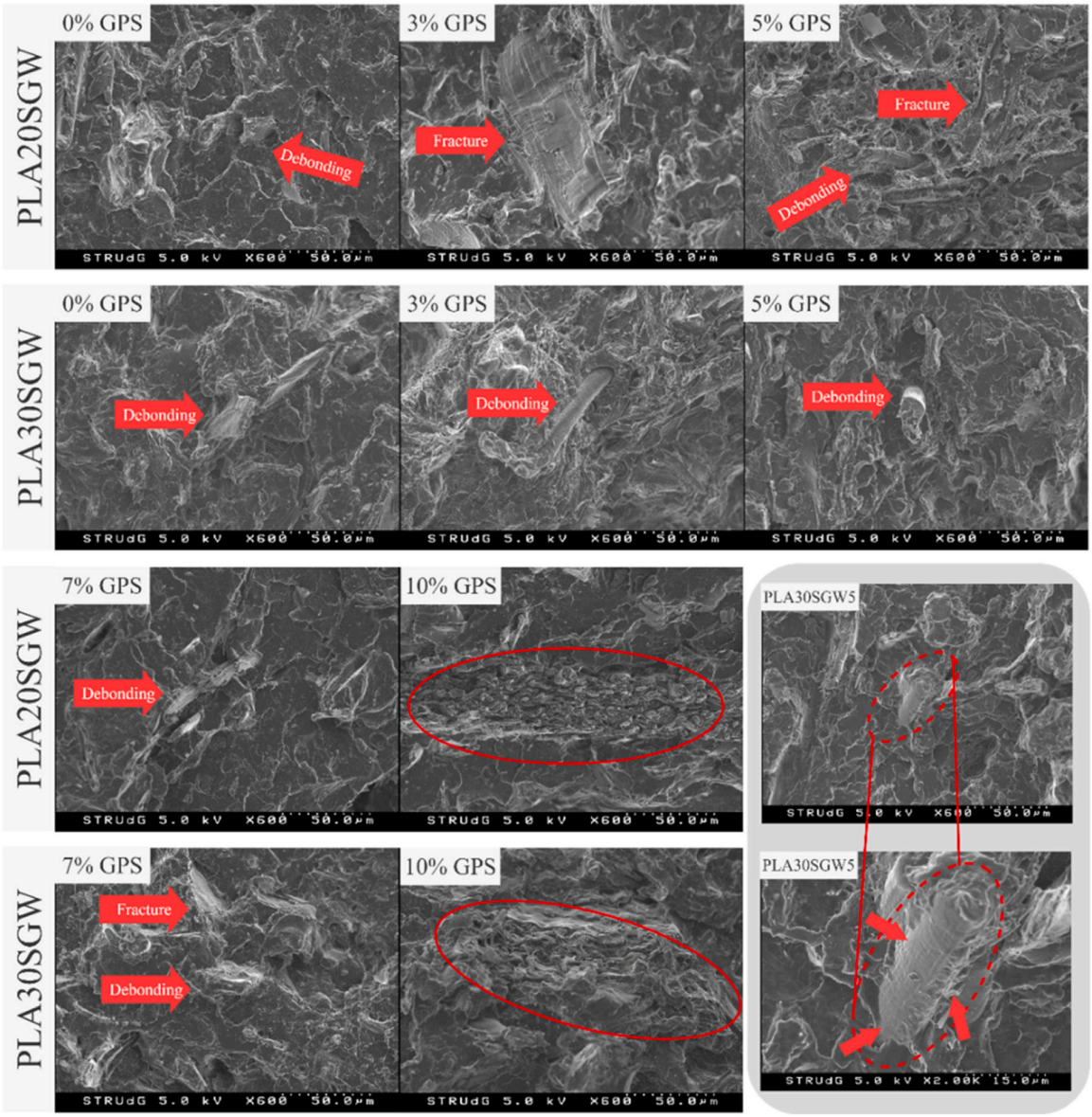

Fig. 6. FE-SEM images of PLA/SGW composites at increasing GPS content.

and an efficient stress transfer between the fiber and the matrix (Doan et al., 2012).

Nandi and Das (2023) reported improvements in the tensile strength of PLA reinforced with 50 wt% Himalayan nettle fibers by 13.33, 18.65, 16.50, and 12.27 % with the presence of 0.5, 1.0, 2.5, and 5.0 % silane coupling agent, respectively. A decrease in tensile strength was observed at high concentrations due to the potential disruption of cellulose crystalline regions. This effect was also observed for biocomposites containing fibers with GPS contents above 7 %. However, the obtained values were still higher than that corresponding to the neat fiber, both at 20 and 30 wt% SGW content. This could also be attributed to the presence of self-condensation structures of silanol groups grafted onto the SGW surface, leading to fiber aggregation. Jandas et al. (2011) enhanced the tensile strength of PLA reinforced with 10, 20, 30, and 40 wt% banana fibers. The best results were obtained with the incorporation of 30 wt% banana fibers. Also, an increase of approximately 15 and 35 % in tensile strength, and 4 and 13 % in tensile modulus upon treatment with two different silane coupling agents, 3-aminopropyltriethoxysilane (APS) and bis-(3-triethoxysilylpropyl) tetrasulfane (Si69), respectively. The Young's modulus of the obtained PLA/SGW biocomposites was significantly enhanced compared to the neat matrix, achieving an average increase of 36 and 79 % for a 20 and 30 wt% SGW addition, respectively, with no clear influence of the GPS content. As mentioned above, Young's modulus is less influenced by fiber-matrix interactions than other properties such as tensile strength, and more related to aspect ratio, fiber stiffness and both fiber distribution and dispersion within the polymer matrix (Ku et al., 2011). In addition, other authors observed no significant effect of coupling agents on the elastic modulus (Bartos et al., 2021; Ramachandran et al., 2022). In another work, Dominguez-Candela et al. (2022) reported an increase in tensile strength with the incorporation of 15 wt% GPS-treated chia seed flour particles into PLA, with an enhancement of 19.2 %.

Compared to neat PLA, SGW-reinforced composites exhibited a reduction ranging from 10 % to 15 % in elongation at break when stiffness was increased (Table 2). This phenomenon is attributed to the decreased deformability of stiff materials, resulting in diminished fracture resistance and intrinsic ductility. Moreover, the incorporation of SGW limited the macromolecular mobility of the PLA matrix chain, thereby impacting the deformability of the composites (Asaithambi et al., 2014). Furthermore, the elongation at break of natural

Table 3
Mean FTSF, E_t^F, σ_t^F and f_c computed by the mRoM and the Hirsch models.

GPS (wt%)	E_t^F (GPa)	σ_t^F (MPa)	FTSF (MPa)	f_c
0			117.52	0.15
3			125.66	0.16
5	27.18 ± 4.01	768.91 ± 37.39	144.61	0.19
7			144.64	0.19
10			134.09	0.17

fiber-reinforced composites is influenced by factors such as fiber entanglement and orientation. In comparison to PLA/jute fiber composites, for instance, PLA/SGW composites demonstrated lower Young's modulus and exhibited a lesser effect on elongation at break (Delgado-Aguilar et al., 2018).

Fig. 6 shows the tensile fractured surface morphology of the PLA/SGW composites analyzed by field emission scanning electron microscope, and the effect of the GPS coupling agent treatment on the tensile properties. In general, SGW fibers during the tensile deformation disposed of two main behaviors, fiber debonding or pullout in which the fiber was detached from the matrix while maintaining its diameter, or fracture and delamination in which the fiber length is ruptured. However, despite the regular fiber failure, its impregnation in the PLA matrix provides a good homogeneity between PLA/fiber, since the incorporation of 20 and 30 wt% SGW increased the tensile strength, showing a good interfacial adhesion of the composites without undergoing silane treatment. The silane coupling agent effect was better elucidated in PLA30SGW5 images with a two-thousandfold magnification (15 μm), where a strong interaction between the PLA matrix and SGW fibers was observed without the presence of voids, leading to a 37 % increase in tensile strength compared with neat PLA. This confirmed that the silane coupling agent was efficiently bonded to the fiber surface. Since SGW incorporation increases the composite stiffness and decreases the elongation at break, shear yielding of the matrix was not observed in the images.

The presence of silanol self-condensation structures adsorbed onto the SGW surface resulted in fiber aggregation. This was evidenced with a red ellipse in Fig. 6 for PLA20SGW10 and PLA30SGW10, inducing points of failure and early rupture of the sample specimens. The reduction in tensile strength with the increase of up to 8 % GPS was also reported by Yang et al. (2023a), who observed that with the excessive amount of free coupling agent, the interfacial bonding of the composites was affected.

3.3. Micromechanical approach

FTSF has been extensively used for assessing the reinforcing performance of different fibers when incorporated into polymer matrices. It results from the combination of the intrinsic tensile strength of the fiber (σ_t^F) and the coupling factor (f_c). The first parameter is inherently linked to the nature of the reinforcement, and should remain constant regardless the fiber-matrix interface, the fiber dispersion and any other parameter related to composite processing and properties. The second, on the contrary, is a compounded factor referring to fiber orientation and fiber-matrix interactions, represented by χ_1 and χ_2 factors, respectively. Due to the technical difficulties to determine σ_t^F experimentally, FTSF is commonly used for preliminarily assessing the reinforcing performance of a certain class of fibers when used as reinforcement of a specific polymer matrix. It must be noted that, as the interactions between reinforcement and matrix influence f_c, the FTSF value will vary from one matrix to another despite the same fiber is used. Furthermore, V^F can also influence this value, as fiber dispersion may be influenced by the fiber loading. However, the effect of fiber content is residual compared to σ_t^F and f_c, and most of the existing literature provides a mean FTSF value regardless V^F. Table 3 shows the obtained mean FTSF as function of the GPS content.

Table 4
Micromechanical parameters of PLA/SGW composites at increasing SGW and GPS content.

GPS (wt%)	V^F	τ_T (MPa)	τ_{VM} (MPa)	L_c^F (μm)	χ_1*	χ_2*
0	0.151	30.47	35.18	312	0.344	0.432
	0.229	33.89	39.13	276		
3	0.151	31.13	35.94	296	0.386	0.379
	0.229	34.18	39.47	280		
5	0.151	33.08	38.19	283	0.388	0.442
	0.229	36.60	42.26	243		
7	0.151	32.43	37.45	294	0.376	0.523
	0.229	37.11	42.85	249		
10	0.151	32.30	37.29	290	0.353	0.542
	0.229	34.45	39.77	271		

* Calculated using the Von Misses criterion.

As detailed above, the FTSF is a compounded factor resulting from σ_t^F and f_c. However, due to the inaccuracy of the single-fiber tensile test for determining the intrinsic tensile strength of the fibers, standard deviations of around 25 % are normally reported (Islam et al., 2011). Alternatively, the Hirsch model can provide useful insights for its determination, assuming that fibers and composite experience the same strain at break (Bowyer and Bader, 1972). The Hirsch model allows the theoretical calculation of the intrinsic Young's modulus of the fiber (E_t^F) by assigning a value of 0.4 to the orientation and stress concentration (β), as widely reported. Then, σ_t^F can be easily calculated and computed together with the FTSF, leading to an estimated f_c as function of the GPS content (Table 3).

The obtained σ_t^F is of the same order of magnitude than in previous works where SGW fibers were used as thermoplastic reinforcement of polypropylene (PP) in presence of maleated polypropylene (MAPP) as the coupling agent (López et al., 2011). Regarding the f_c values of Table 3, the GPS content appeared to directly influence the interactions between the reinforcement and the polymer matrix, gradually increasing from 0.15 (unmodified SGW) to 0.19 (5 and 7 % GPS) to later decrease to 0.17. Surprisingly, the obtained E_t^F of 27.18 GPa was significantly higher than the previously reported value of 18.2 GPa for the situation in which SGW fibers were used for PP reinforcement. This higher E_t^F can be attributed to the highest rigidity of the PLA matrix, which may have influenced the calculations. Considering the low strain at break of the composites, compared to SGW-reinforced PP composites, this higher value was expected. Considering that the intrinsic tensile strength of the fibers is an inherent property and that, theoretically, it must remain constant regardless the system where fibers are embedded, any change on the FTSF must come from the coupling factor, indicating that interface and orientation exerts a determining role in the fiber reinforcing capacity within the polymer matrix. The obtained f_c value indicates that composites prepared from SGW modified with GPS contents ranging from 5 % to 7 % leverage systems with appropriate fiber-matrix interactions. Actually, for randomly oriented fiber-reinforced composites, a coupling factor of 0.20 is an indicator of well-bonded systems. As previously discussed, f_c results from the combination between fiber orientation and fiber-matrix interfacial features. The interfacial shear stress (IFSS or τ) can be determined by the Bowyer-Bader iterative solution to the Kelly-Tyson model or, in a more simplified scenario, estimated according to the Tresca and/or Von Misses criteria (τ_T and τ_{VM}, respectively). This allows for the determination of the critical length (L_c^F) if σ_t^F and fiber diameter (d^F) computed together, as described by Eq. 7. Critical length varied from one composite to another, but all values ranged from 242 to 311 μm. In addition, considering the average fiber length weighted in length (Table 1) of the fibers after the extraction process, this is preserving the fiber morphology within the composite, it seems that fibers could be generally considered as subcritical. A more detailed analysis could be performed by considering the fiber length distribution, as previously reported in other studies (Espinach et al., 2024; Tarrés et al., 2018). However, this

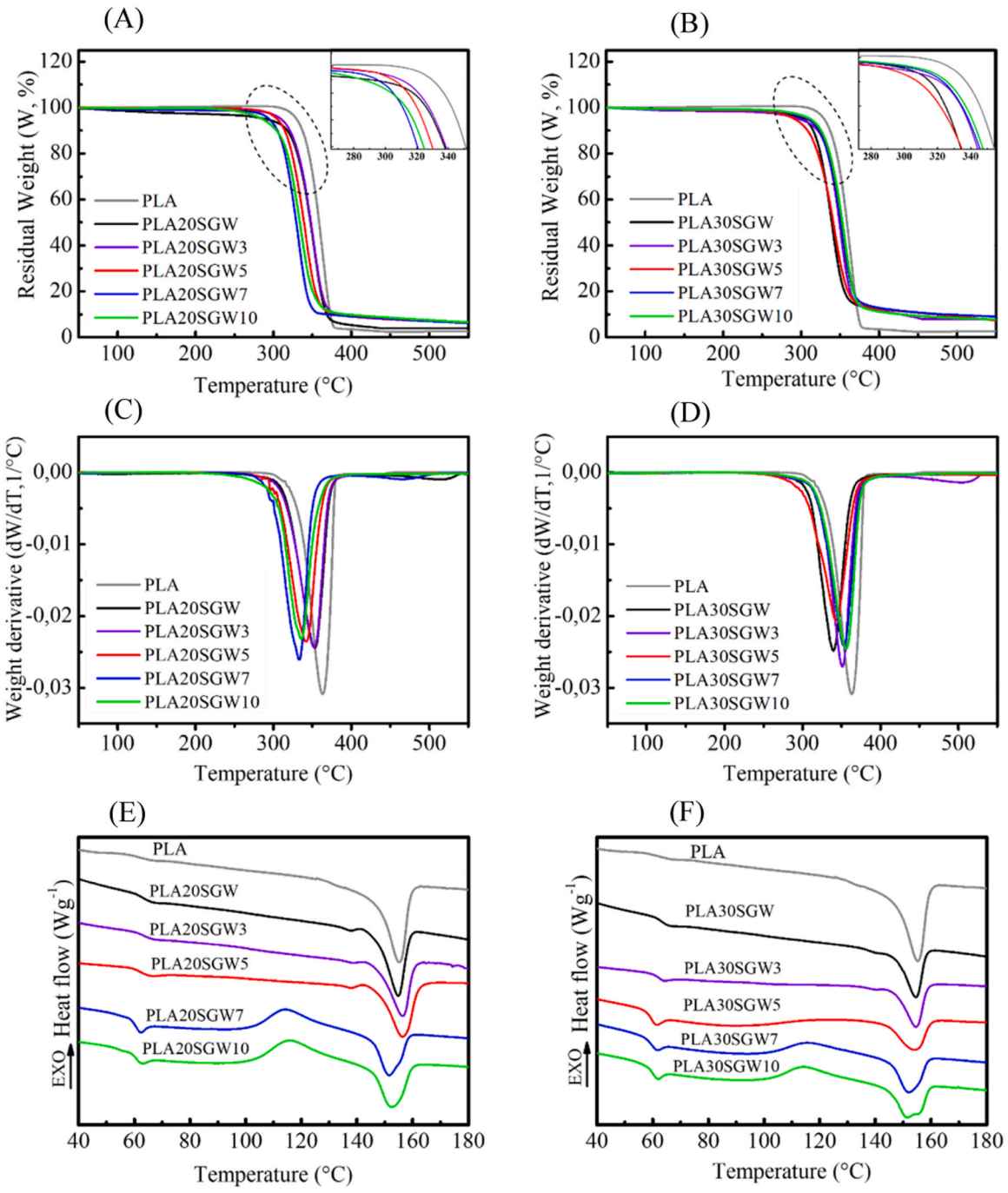

Fig. 7. TGA (A, B) and DTG (C, D) measurements of the biocomposites reinforced with 20 and 30 % wt of SGW; DSC thermograms of (E) PLA20SGW and (F) PLA30SGW composites.

simplified methodology allows the understanding of the mechanisms taking place during fiber reinforcement of PLA. In this sense, χ_2 can be obtained from Eq. 8, and χ_1 can be easily obtained considering the obtained values of f_c. Table 4 provides the average values of these micromechanical parameters in relation to the GPS content.

As depicted from Table 4, the interface factor χ_2 exhibited an increasing tendency with the GPS content. This is aligned with the previously observed reduction of O-H stretching vibrations by FTIR, potentially generating bonds between lignocellulosic hydroxyl groups and silanol groups that, by hindering intra- and interfiber hydrogen bonding, enhance the fiber-matrix interactions with PLA. The fiber orientation factor χ_1 revealed values between 0.344 and 0.388. According to the literature, a value of 3/8 (0.375) for the orientation factor can be considered for randomly oriented 2D composites, which is a comparable case to the composites under study due to the thickness of the injected specimens (Garkhail et al., 2000; Thomason et al., 1996). In any case, the micromechanical analysis reveals that both 5 and 7 % GPS addition provides a good orientation and interface between PLA and SGW, which is aligned with the macromechanical study of the tensile strength.

3.4. Thermal characterization of biocomposites

The thermal degradation behavior and stability of the biocomposites reinforced with untreated and silane-treated SGW fibers are shown in Fig. 7, while Table 5 summarizes the composites' thermal parameters.

Table 5
TGA/DTG and DSC thermal properties of neat PLA and PLA/SGW biocomposites.

Sample	T_i*	T_{max}	T_f	R	T_g	T_{cc}	T_c	T_m	ΔH_{cc}	ΔH_m	X_c
	(°C)			(%)	(°C)				(Jg^{-1})		(%)
PLA	330	363	380	2.5	60.6	-	-	155	-	34.9	37.3
PLA20SGW	290	353	374	4.2	59.9	-	-	145	2.1	22.6	27.4
PLA20SGW3	310	352	372	7.1	65.7	-	-	155	1.9	20.1	25.3
PLA20SGW5	304	342	370	7.3	65.1	123	128	155	1.8	21.3	26.1
PLA20SGW7	294	333	351	7.6	60.1	103	114	151	12.1	18.0	7.9
PLA20SGW10	285	335	360	7.5	60.7	103	116	152	14.0	20.0	8.0
PLA30SGW	303	340	360	9.2	64.5	-	-	155	1.4	17.1	24.0
PLA30SGW3	297	350	385	7.9	62.5	-	-	154	1.5	15.2	20.9
PLA30SGW5	291	347	395	9.4	59.5	100	114	151	1.6	15.8	21.6
PLA30SGW7	307	356	388	10.0	59.6	102	115	152	7.5	15.2	11.8
PLA30SGW10	311	358	383	9.1	59.7	103	114	151	8.3	15.7	11.3

* Considering 95 % residue.

Both TGA and DTG thermograms (Fig. 7, A to D) show that neat PLA and PLA/SGW biocomposites decomposed in a single step. The initial (T_i) and the maximum degradation temperature (T_{max}) of PLA was decreased by the nontreated SGW fiber incorporation. The presence of lignocellulosic fibers affects the thermal stability of polymeric composites, decreasing the onset temperature due to the lower degradation temperature of cellulose, hemicelluloses, and lignin (Eselini et al., 2020; Fang et al., 2022; Jandas et al., 2011; Ozyhar et al., 2020). However, for the silane-treated 20 wt% SGW fibers (Fig. 7, A and B), the addition of 3 and 5 wt% of the coupling agent was able to increase T_i and decrease both $T_{max,}$ and the final degradation temperature (T_f). By contrast, the 3 and 5 wt% silane-treated 30 wt% SGW fibers suffered a decrease in T_i and T_{max}, but a significant increase in T_f.

Figs. 7D and 7E show an increment in the maximum degradation rate of the silane-treated PLA30SGW, indicating improvements of the composite's thermal stability. Hence, the silane coupling fiber treatment was able to raise the PLA/SGW interfacial adhesion. The presence of a greater lignin content in the composites, due to the use of higher fiber contents (*e.g.*, 30 wt% SGW), required more energy for the material degradation, since lignin tends to degrade at higher temperatures, suggesting better adhesion and interaction among the GPS coupling agent, lignin, and the PLA matrix (Fang et al., 2022; Wang et al., 2020).

The effect of fiber incorporation and coupling agent treatment on the biocomposite's thermal behavior was assessed by DSC. The thermograms of Fig. 7E and 7F present a single glass transition temperature (T_g) for all samples, ranging from 59 to 66 °C, as described in Table 5. An increment in the T_g was observed for PLA20SGW3, PLA20SGW5, PLA30SGW, and PLA30SGW3, indicating an improvement in the composite's thermal stability by an increase in the fiber-polymer entanglement, while other samples remained like neat PLA.

With the increase in GPS content from 7 to 10 wt%, a cold-crystallization phenomenon was observed for both fiber contents, presenting cold-crystallization temperatures (T_{cc}) between 100 and 123 °C and crystallization (T_c) between 114 and 128 °C. This corroborates that the silane coupling agent promoted the recrystallization of PLA chains upon heating, promoting molecular entanglement by acting as a nucleating agent due to its epoxy group linkage with the PLA matrix (Chun et al., 2012). While the PLA melting temperature (T_m) was measured as a single peak at 155 °C, the incorporation of 20 wt% SGW decreased it to 145 °C. However, T_m remained unchanged at 155 °C for 30 wt% SGW. As the presence of 7–10 wt% GPS affected both T_{cc} and T_c of PLA, the melting temperature was also changed, displaying a double melting peak and a decrease in the melting enthalpy (ΔH_m).

Regarding the degree of crystallinity (X_c), the neat PLA showed 37.3 % crystalline structure, which was reduced to 27.4 % and 24.0 % with the incorporation of 20 and 30 wt% SGW, respectively, decreasing the nucleation activity of these composites (Table 5). Slight modifications in the crystallinity were observed for the silane-treated composites with 3 and 5 wt% GPS. However, by increasing the GPS content to 7 and 10 wt %, the composite's crystallinity decreased to around 70 % for the 20 wt % SGW and to around 50 % for the 20 wt% SGW. The generation of mobility restrictions in the polymer by the higher content of the coupling agent led to a rearrangement of chains, hampering nucleation and crystal growth, and unexpectedly decreasing the composite's degree of crystallinity. This was also related to the presence of a cold crystallization peak in these samples, which arises from the reorganization of amorphous domains into crystalline regions on account of the increased macromolecular flexibility upon a temperature increase during the analysis (Jandas et al., 2011).

4. Conclusions

The present work shows the feasibility of incorporating a high-yield mechanical pulp into PLA for the development of high-performance biocomposites through the partial modification of the fibers by means of a silane-coupling strategy. While a moderate increase in the tensile strength was found with the addition of 20 and 30 wt% SGW, accounting for 14 and 27 %, respectively, this enhancement was further increased when fibers were partially modified with GPS. Concretely, the biocomposites reinforced with 30 wt% SGW and modified with 5 and 7 wt % GPS revealed a tensile strength enhancement of 37.4 and 39.3 %, respectively. This was attributed to an improvement in the PLA-SGW interface, as well as to an appropriate dispersion of the fibers within the polymer matrix. Actually, the micromechanical modelling revealed coupling factors of around 0.2, which have been previously reported for well-bonded systems. These biocomposites stand out as a competitive alternative to commodity GF composites, such is the case of GF-reinforced PP, while exhibiting a much lower density. Although the inclusion of SGW influenced the rheological features of PLA, the obtained biocomposites were found to be processable, as revealed by the MFI measurements. There was an increase in complex viscosity and a reduction in the loss factor, suggesting a predominantly elastic behavior. In addition, thermal stability was slightly improved, although no significant changes were found in the thermal properties of the biocomposites compared to neat PLA.

CRediT authorship contribution statement

Roberto J. Aguado: Writing – review & editing, Methodology, Investigation. **Giulia Herbst:** Writing – original draft, Methodology, Investigation, Conceptualization. **Marc Delgado-Aguilar:** Writing – review & editing, Validation, Supervision, Formal analysis, Conceptualization. **Luiz P. Ramos:** Writing – review & editing, Funding acquisition. **Pere Mutjé:** Validation, Supervision, Methodology. **Quim Tarrés:** Methodology, Investigation. **Marcos L. Corazza:** Writing – review & editing, Funding acquisition.

Declaration of Competing Interest

The authors declare that they have no known competing financial

interests or personal relationships that could have appeared to influence the work reported in this paper.

Data Availability

Data will be made available on request.

Acknowledgments

The authors wish to acknowledge the financial support of the Coordenação de Aperfeiçoamento de Pessoal de Nível Superior – Brazil (CAPES) – Finance Code 001 for the mobility program granted to Giulia Herbst, and the Conselho Nacional de Desenvolvimento Científico e Tecnológico (CNPq, Brazil) with the Programa de Mestrado e Doutorado Acadêmico para Inovação MAI/DAI and Earth Renewable Technologies BR LTDA as a partnership. Marc Delgado-Aguilar and Quim Tarrés are Serra Húnter Fellows.

References

Agarwal, J., Sahoo, S., Mohanty, S., Nayak, S.K., 2020. Progress of novel techniques for lightweight automobile applications through innovative eco-friendly composite materials: a review. J. Thermoplast. Compos. Mater. 33, 978–1013. https://doi.org/10.1177/0892705718815530.

Ali, S.S., Abdelkarim, E.A., Elsamahy, T., Al-Tohamy, R., Li, F., Kornaros, M., Zuorro, A., Zhu, D., Sun, J., 2023. Bioplastic production in terms of life cycle assessment: a state-of-the-art review. Environ. Sci. Ecotechnol. 15, 100254 https://doi.org/10.1016/j.ese.2023.100254.

Arslan, C., Dogan, M., 2018. The effects of silane coupling agents on the mechanical properties of basalt fiber reinforced poly(butylene terephthalate) composites. Compos B Eng. 146, 145–154. https://doi.org/10.1016/j.compositesb.2018.04.023.

Asaithambi, B., Ganesan, G., Ananda Kumar, S., 2014. Bio-composites: development and mechanical characterization of banana/sisal fibre reinforced poly lactic acid (PLA) hybrid composites. Fibers Polym. 15, 847–854. https://doi.org/10.1007/s12221-014-0847-y.

Awal, A., Rana, M., Sain, M., 2015. Thermorheological and mechanical properties of cellulose reinforced PLA bio-composites. Mech. Mater. 80, 87–95. https://doi.org/10.1016/j.mechmat.2014.09.009.

Balla, V.K., Kate, K.H., Satyavolu, J., Singh, P., Tadimeti, J.G.D., 2019. Additive manufacturing of natural fiber reinforced polymer composites: processing and prospects. Compos B Eng. 174, 106956 https://doi.org/10.1016/j.compositesb.2019.106956.

Barczewski, M., Matykiewicz, D., Szostak, M., 2020. The effect of two-step surface treatment by hydrogen peroxide and silanization of flax/cotton fabrics on epoxy-based laminates thermomechanical properties and structure. J. Mater. Res. Technol. 9, 13813–13824. https://doi.org/10.1016/j.jmrt.2020.09.120.

Bartos, A., Nagy, K., Anggono, J., Antoni, Purwaningsih, H., Móczó, J., Pukánszky, B., 2021. Biobased PLA/sugarcane bagasse fiber composites: effect of fiber characteristics and interfacial adhesion on properties. Compos. Part A Appl. Sci. Manuf. 143 https://doi.org/10.1016/j.compositesa.2021.106273.

Bhong, M., Khan, T.K.H., Devade, K., Vijay Krishna, B., Sura, S., Eftikhaar, H.K., Pal Thethi, H., Gupta, N., 2023. Review of composite materials and applications. Mater. Today Proc. https://doi.org/10.1016/j.matpr.2023.10.026.

Bianchi, S., Thömen, H., Junginger, S., Pichelin, F., 2019. Medium density boards made of groundwood fibres: an analysis of their mechanical and physical properties. Eur. J. Wood Wood Prod. 77, 71–77. https://doi.org/10.1007/s00107-018-1367-z.

Birnin-Yauri, A.U., Ibrahim, N.A., Zainuddin, N., Abdan, K., Then, Y.Y., Chieng, B.W., 2016. Influence of kenaf core fiber incorporation on the mechanical performance and dimensional stability of oil palm fiber reinforced poly(lactic acid) hybrid biocomposites. Bioresources 11, 3332–3355. https://doi.org/10.15376/biores.11.2.3332-3355.

Bowyer, W.H., Bader, M.G., 1972. On the re-inforcement of thermoplastics by imperfectly aligned discontinuous fibres. J. Mater. Sci. 7, 1315–1321. https://doi.org/10.1007/BF00550698.

Chatziparaskeva, G., Papamichael, I., Voukkali, I., Loizia, P., Sourkouni, G., Argirusis, C., Zorpas, A.A., 2022. End-of-life of composite materials in the framework of the circular economy. Microplastics 1, 377–392. https://doi.org/10.3390/microplastics1030028.

Chen, K., Li, P., Li, Xingong, Liao, C., Li, Xianjun, Zuo, Y., 2021. Effect of silane coupling agent on compatibility interface and properties of wheat straw/polylactic acid composites. Int. J. Biol. Macromol. 182, 2108–2116. https://doi.org/10.1016/j.ijbiomac.2021.05.207.

Chun, K.S., Husseinsyah, S., Osman, H., 2012. Mechanical and thermal properties of coconut shell powder filled polylactic acid biocomposites: effects of the filler content and silane coupling agent. J. Polym. Res. 19 https://doi.org/10.1007/s10965-012-9859-8.

Dammak, M., Fourati, Y., Tarrés, Q., Delgado-Aguilar, M., Mutjé, P., Boufi, S., 2020. Blends of PBAT with plasticized starch for packaging applications: mechanical properties, rheological behaviour and biodegradability. Ind. Crops Prod. 144, 112061 https://doi.org/10.1016/j.indcrop.2019.112061.

de Buyl, F., Kretschmer, A., 2008. Understanding hydrolysis and condensation kinetics of γ-Glycidoxypropyltrimethoxysilane. J. Adhes. 84, 125–142. https://doi.org/10.1080/00218460801952809.

del Angel-Monroy, M., Escobar-Barrios, V., Peña-Juarez, M.G., Lugo-Uribe, L.E., Navarrete-Damian, J., Perez, E., Gonzalez-Calderon, J.A., 2024. Effect of coconut fibers chemically modified with alkoxysilanes on the crystallization, thermal, and dynamic mechanical properties of poly(lactic acid) composites. Polym. Bull. 81, 843–870. https://doi.org/10.1007/s00289-023-04740-6.

Delgado-Aguilar, M., Oliver-Ortega, H., Alberto Méndez, J., Camps, J., Espinach, F.X., Mutjé, P., 2018. The role of lignin on the mechanical performance of polylactic acid and jute composites. Int J. Biol. Macromol. 116, 299–304. https://doi.org/10.1016/j.ijbiomac.2018.04.124.

Delogu, M., Zanchi, L., Dattilo, C.A., Pierini, M., 2017. Innovative composites and hybrid materials for electric vehicles lightweight design in a sustainability perspective. Mater. Today Commun. 13, 192–209. https://doi.org/10.1016/j.mtcomm.2017.09.012.

Doan, T.T.L., Brodowsky, H., Mäder, E., 2012. Jute fibre/epoxy composites: surface properties and interfacial adhesion. Compos Sci. Technol. 72, 1160–1166. https://doi.org/10.1016/j.compscitech.2012.03.025.

Dominguez-Candela, I., Gomez-Caturla, J., Cardona, S.C., Lora-García, J., Fombuena, V., 2022. Novel compatibilizers and plasticizers developed from epoxidized and maleinized chia oil in composites based on PLA and chia seed flour. Eur. Polym. J. 173, 111289 https://doi.org/10.1016/j.eurpolymj.2022.111289.

Eftekhari, M., Fatemi, A., 2016. Tensile behavior of thermoplastic composites including temperature, moisture, and hygrothermal effects. Polym. Test. 51, 151–164. https://doi.org/10.1016/j.polymertesting.2016.03.011.

El Omari, Y., Yousfi, M., Duchet-Rumeau, J., Maazouz, A., 2023. Interfacial rheology for probing the in-situ chemical reaction at interfaces of molten polymer systems. Mater. Today Commun. 35, 105640 https://doi.org/10.1016/j.mtcomm.2023.105640.

Eselini, N., Tirkes, S., Akar, A.O., Tayfun, U., 2020. Production and characterization of poly (lactic acid)-based biocomposites filled with basalt fiber and flax fiber hybrid. J. Elastomers Plast. 52, 701–716. https://doi.org/10.1177/0095244319884716.

Espinach, F.X., Vilaseca, F., Tarrés, Q., Delgado-Aguilar, M., Aguado, R.J., Mutjé, P., 2024. An alternative method to evaluate the micromechanics tensile strength properties of natural fiber strand reinforced polyolefin composites. The case of hemp strand-reinforced polypropylene. Compos B Eng. 273, 111211 https://doi.org/10.1016/j.compositesb.2024.111211.

Fan, Z., Gao, J., Wu, Y., Yin, D., Chen, S., Tu, H., Wei, T., Zhang, C., Zhu, H., Jin, H., 2023. Highly enhanced mechanical, thermal, and crystallization performance of PLA/PBS composite by glass fiber coupling agent modification. Polym. (Basel) 15, 3164. https://doi.org/10.3390/polym15153164.

Fang, X., Li, Y., Zhao, J., Xu, J., Li, C., Liu, J., Liu, Y., Guo, H., 2022. Improved interfacial performance of bamboo fibers/polylactic acid composites enabled by a self-supplied bio-coupling agent strategy. J. Clean. Prod. 380, 134719 https://doi.org/10.1016/j.jclepro.2022.134719.

Ferraz, A., Baeza, J., Rodriguez, J., Freer, J., 2000. Estimating the chemical composition of biodegraded pine and eucalyptus wood by DRIFT spectroscopy and multivariate analysis. Bioresour. Technol. 74, 201–212.

Fourati, Y., Tarrés, Q., Delgado-Aguilar, M., Mutjé, P., Boufi, S., 2021. Cellulose nanofibrils reinforced PBAT/TPS blends: Mechanical and rheological properties. Int. J. Biol. Macromol. 183, 267–275. https://doi.org/10.1016/j.ijbiomac.2021.04.102.

Garkhail, S.K., Heijenrath, R.W.H., Peijs, T., 2000. Mechanical properties of natural-fibre-mat-reinforced thermoplastics based on flax fibres and polypropylene. Appl. Compos. Mater. 7, 351–372. https://doi.org/10.1023/A:1026590124038.

Gonçalves, R.M., Martinho, A., Oliveira, J.P., 2022. Recycling of reinforced glass fibers waste: current status. Materials 15, 1596. https://doi.org/10.3390/ma15041596.

Granda, L.A., Espinach, F.X., Tarrés, Q., Méndez, J.A., Delgado-Aguilar, M., Mutjé, P., 2016a. Towards a good interphase between bleached kraft softwood fibers and poly (lactic) acid. Compos. B Eng. 99, 514–520. https://doi.org/10.1016/j.compositesb.2016.05.008.

Granda, L.A., Espinach, F.X., Tarrés, Q., Méndez, J.A., Delgado-Aguilar, M., Mutjé, P., 2016b. Towards a good interphase between bleached kraft softwood fibers and poly (lactic) acid. Compos. B Eng. 99, 514–520. https://doi.org/10.1016/j.compositesb.2016.05.008.

Graupner, N., Schmidt, S., Gauss, C., Müssig, J., 2023. Making positive use of the fibrillation of lyocell fibres in composite materials. Compos. Part C: Open Access 11, 100359. https://doi.org/10.1016/j.jcomc.2023.100359.

Gurunathan, T., Mohanty, S., Nayak, S.K., 2015. A review of the recent developments in biocomposites based on natural fibres and their application perspectives. Compos. Part A Appl. Sci. Manuf. 77, 1–25. https://doi.org/10.1016/j.compositesa.2015.06.007.

Hakim, R.H., Cailloux, J., Santana, O.O., Bou, J., Sánchez-Soto, M., Odent, J., Raquez, J. M., Dubois, P., Carrasco, F., Maspoch, M.L., 2017. PLA/SiO2 composites: influence of the filler modifications on the morphology, crystallization behavior, and mechanical properties. J. Appl. Polym. Sci. 134 https://doi.org/10.1002/app.45367.

Hasan, A., Rabbi, M.S., Maruf Billah, M., 2022. Making the lignocellulosic fibers chemically compatible for composite: a comprehensive review. Clean. Mater. 4, 100078 https://doi.org/10.1016/j.clema.2022.100078.

Hietala, M., Rollo, P., Kekäläinen, K., Oksman, K., 2014. Extrusion processing of green biocomposites: compounding, fibrillation efficiency, and fiber dispersion. J. Appl. Polym. Sci. 131 https://doi.org/10.1002/app.39981.

Hristov, V., Vlachopoulos, J., 2007. Influence of coupling agents on melt flow behavior of natural fiber composites. Macromol. Mater. Eng. 292, 608–619. https://doi.org/10.1002/mame.200600459.

Islam, M.S., Pickering, K.L., Foreman, N.J., 2011. Influence of alkali fiber treatment and fiber processing on the mechanical properties of hemp/epoxy composites. J. Appl. Polym. Sci. 119, 3696–3707. https://doi.org/10.1002/app.31335.
Jalaee, A., Foster, E.J., 2024. Improvement in the thermomechanical properties and adhesion of wood fibers to the polyamide 6 matrix by sequential ball milling technique. ACS Sustain. Chem. Eng. 12, 490–500. https://doi.org/10.1021/acssuschemeng.3c06351.
Jandas, P.J., Mohanty, S., Nayak, S.K., Srivastava, H., 2011. Effect of surface treatments of banana fiber on mechanical, thermal, and biodegradability properties of PLA/banana fiber biocomposites. Polym. Compos. 32, 1689–1700. https://doi.org/10.1002/pc.21165.
Javier-Astete, R., Jimenez-Davalos, J., Zolla, G., 2021. Determination of hemicellulose, cellulose, holocellulose and lignin content using FTIR in Calycophyllum spruceanum (Benth.) K. Schum. And Guazuma crinita Lam. PLoS One 16, 1–12. https://doi.org/10.1371/journal.pone.0256559.
Joshi, S.V., Drzal, L.T., Mohanty, A.K., Arora, S., 2004. Are natural fiber composites environmentally superior to glass fiber reinforced composites? Compos. Part A Appl. Sci. Manuf. 35, 371–376. https://doi.org/10.1016/j.compositesa.2003.09.016.
Kılıç, E., Fullana-i-Palmer, P., Fullana, M., Delgado-Aguilar, M., Puig, R., 2024. Circularity of new composites from recycled high density polyethylene and leather waste for automotive bumpers. Testing performance and environmental impact. Sci. Total Environ. 919, 170413 https://doi.org/10.1016/j.scitotenv.2024.170413.
Kossentini Kallel, T., Taktak, R., Guermazi, N., Mnif, N., 2018. Mechanical and structural properties of glass fiber-reinforced polypropylene (PPGF) composites. Polym. Compos. 39, 3497–3508. https://doi.org/10.1002/pc.24369.
Ku, H., Wang, H., Pattarachaiyakoop, N., Trada, M., 2011. A review on the tensile properties of natural fiber reinforced polymer composites. Compos. B Eng. 42, 856–873. https://doi.org/10.1016/j.compositesb.2011.01.010.
La Mantia, F.P., Morreale, M., 2011. Green composites: a brief review. Compos. Part A Appl. Sci. Manuf. 42, 579–588. https://doi.org/10.1016/j.compositesa.2011.01.017.
Lee, C.H., Khalina, A., Lee, S.H., 2021. Importance of interfacial adhesion condition on characterization of plant-fiber-reinforced polymer composites: a review. Polym. (Basel) 13, 438. https://doi.org/10.3390/polym13030438.
Li, M., Pu, Y., Thomas, V.M., Yoo, C.G., Ozcan, S., Deng, Y., Nelson, K., Ragauskas, A.J., 2020. Recent advancements of plant-based natural fiber–reinforced composites and their applications. Compos. B Eng. 200, 108254 https://doi.org/10.1016/j.compositesb.2020.108254.
Liu, Y., Lv, X., Bao, J., Xie, J., Tang, X., Che, J., Ma, Y., Tong, J., 2019. Characterization of silane treated and untreated natural cellulosic fibre from corn stalk waste as potential reinforcement in polymer composites. Carbohydr. Polym. 218, 179–187. https://doi.org/10.1016/j.carbpol.2019.04.088.
Long, H., Wu, Z., Dong, Q., Shen, Y., Zhou, W., Luo, Y., Zhang, C., Dong, X., 2019. Effect of polyethylene glycol on mechanical properties of bamboo fiber-reinforced polylactic acid composites. J. Appl. Polym. Sci. 136 https://doi.org/10.1002/app.47709.
López, J.P., Méndez, J.A., El Mansouri, N.-E., Mutjé, P., Vilaseca, F., 2011. Mean intrinsic tensile properties of stone groundwood fibers from softwood. Bioresources 6, 5037–5049. https://doi.org/10.15376/biores.6.4.5037-5049.
López, J.P., Méndez, J.A., Espinach, F.X., Julián, F., Mutjé, P., Vilaseca, F., 2012. Tensile strength characteristics of polypropylene composites reinforced with stone groundwood fibers from softwood. Bioresources 7, 3188–3200. https://doi.org/10.15376/biores.7.3.3188-3200.
Luo, H., Zhang, C., Xiong, G., Wan, Y., 2016. Effects of alkali and alkali/silane treatments of corn fibers on mechanical and thermal properties of its composites with polylactic acid. Polym. Compos. 37, 3499–3507. https://doi.org/10.1002/pc.23549.
Maaoui, A., Ben Hassen Trabelsi, A., Ben Abdallah, A., Chagtmi, R., Lopez, G., Cortazar, M., Olazar, M., 2023. Assessment of pine wood biomass wastes valorization by pyrolysis with focus on fast pyrolysis biochar production. J. Energy Inst. 108, 101242 https://doi.org/10.1016/j.joei.2023.101242.
Madhavan Nampoothiri, K., Nair, N.R., John, R.P., 2010. An overview of the recent developments in polylactide (PLA) research. Bioresour. Technol. 101, 8493–8501. https://doi.org/10.1016/j.biortech.2010.05.092.
Méndez, J.A., Vilaseca, F., Pèlach, M.A., López, J.P., Barberà, L., Turon, X., Gironès, J., Mutjé, P., 2007. Evaluation of the reinforcing effect of ground wood pulp in the preparation of polypropylene-based composites coupled with maleic anhydride grafted polypropylene. J. Appl. Polym. Sci. 105, 3588–3596. https://doi.org/10.1002/app.26426.
Mujtaba, M., Fernandes Fraceto, L., Fazeli, M., Mukherjee, S., Savassa, S.M., Araujo de Medeiros, G., do Espírito Santo Pereira, A., Mancini, S.D., Lipponen, J., Vilaplana, F., 2023. Lignocellulosic biomass from agricultural waste to the circular economy: a review with focus on biofuels, biocomposites and bioplastics. J. Clean. Prod. 402, 136815 https://doi.org/10.1016/j.jclepro.2023.136815.
Mutjé, P., Vallejos, M.E., Gironès, J., Vilaseca, F., López, A., López, J.P., Méndez, J.A., 2006. Effect of maleated polypropylene as coupling agent for polypropylene composites reinforced with hemp strands. J. Appl. Polym. Sci. 102, 833–840. https://doi.org/10.1002/app.24315.
Nandi, P., Das, D., 2023. Mechanical, thermo-mechanical and biodegradation behaviour of surface-silanized nettle fabric-reinforced poly(lactic acid) composites. Mater. Chem. Phys. 297, 127381 https://doi.org/10.1016/j.matchemphys.2023.127381.
Ozyhar, T., Baradel, F., Zoppe, J., 2020. Effect of functional mineral additive on processability and material properties of wood-fiber reinforced poly(lactic acid) (PLA) composites. Compos Part A Appl. Sci. Manuf. 132, 105827 https://doi.org/10.1016/j.compositesa.2020.105827.
Pang, X., Zhuang, X., Tang, Z., Chen, X., 2010. Polylactic acid (PLA): research, development and industrialization. Biotechnol. J. 5, 1125–1136. https://doi.org/10.1002/biot.201000135.
Plastics Europe, 2022Plastics – the Facts: An analysis of European plastics production, demand, conversion and end-of-life management..
Qian, S., Kong, Y., Cheng, H., Tu, S., Zhai, C., 2023. Interfacial interaction improvement of polylactic acid/bamboo-char biocomposites for high toughness, good strength, and excellent thermal stability. Surf. Interfaces 42, 103315. https://doi.org/10.1016/j.surfin.2023.103315.
Ramachandran, A.R., Mavinkere Rangappa, S., Kushvaha, V., Khan, A., Seingchin, S., Dhakal, H.N., 2022. Modification of fibers and matrices in natural fiber reinforced polymer composites: a comprehensive review. Macromol. Rapid Commun. 43, 1–38. https://doi.org/10.1002/marc.202100862.
Reyes, P., Mendonça, R.T., Rodríguez, J., Fardim, P., Vega, B., 2013. Characterization of the hemicellulosic fraction obtained after pre-hydrolysis of Pinus radiata wood chips with hot-water at different initial PH. J. Chil. Chem. Soc. 58, 1614–1618. https://doi.org/10.4067/S0717-97072013000100024.
Rodríguez, L.J., Orrego, C.E., Ribeiro, I., Peças, P., 2018. Life-cycle assessment and life-cycle cost study of banana (Musa sapientum) fiber Biocomposite materials. Procedia CIRP 69, 585–590. https://doi.org/10.1016/j.procir.2017.11.145.
Sable, I., Grinfelds, U., Jansons, A., Vikele, L., Irbe, I., Verovkins, A., Treimanis, A., 2012. Comparison of the properties of wood and pulp fibers from lodgepole pine (Pinus contorta) and scots pine (Pinus sylvestris). Bioresources 7 (2), 1771–1783. https://doi.org/10.15376/biores.7.2.1771-1783.
Safdari, F., Bagheriasl, D., Carreau, P.J., Heuzey, M.C., Kamal, M.R., 2018. Rheological, mechanical, and thermal properties of polylactide/cellulose nanofiber biocomposites. Polym. Compos. 39, 1752–1762. https://doi.org/10.1002/pc.24127.
Serra-Parareda, F., Vilaseca, F., Aguado, R., Espinach, F.X., Tarrés, Q., Delgado-Aguilar, M., 2021. Effective young's modulus estimation of natural fibers through micromechanical models: the case of henequen fibers reinforced-PP composites. Polym. (Basel) 13, 3947. https://doi.org/10.3390/polym13223947.
Shanmugam, V., Mensah, R.A., Försth, M., Sas, G., Restás, Á., Addy, C., Xu, Q., Jiang, L., Neisiany, R.E., Singha, S., George, G., Jose E, T., Berto, F., Hedenqvist, M.S., Das, O., Ramakrishna, S., 2021. Circular economy in biocomposite development: state-of-the-art, challenges and emerging trends. Compos. Part C: Open Access 5, 100138. https://doi.org/10.1016/j.jcomc.2021.100138.
Siakeng, R., Jawaid, M., Ariffin, H., Sapuan, S.M., Asim, M., Saba, N., 2019. Natural fiber reinforced polylactic acid composites: a review. Polym. Compos. 40, 446–463. https://doi.org/10.1002/pc.24747.
Sikorska, W., Musioł, M., Zawidlak-Węgrzyńska, B., Rydz, J., 2021. End-of-life options for (bio)degradable polymers in the circular economy. Adv. Polym. Technol. 2021, 1–18. https://doi.org/10.1155/2021/6695140.
Tan, Z., Hu, L., Yang, D., Zheng, D., Qiu, X., 2023. Lignin: excellent hydrogel swelling promoter used in cellulose aerogel for efficient oil / water separation. J. Colloid Interface Sci. 629, 422–433. https://doi.org/10.1016/j.jcis.2022.08.185.
Tarrés, Q., Melbø, J.K., Delgado-Aguilar, M., Espinach, F.X., Mutjé, P., Chinga-Carrasco, G., 2018. Bio-polyethylene reinforced with thermomechanical pulp fibers: mechanical and micromechanical characterization and its application in 3D-printing by fused deposition modelling. Compos. B Eng. 153, 70–77. https://doi.org/10.1016/j.compositesb.2018.07.009.
Thomason, J.L., Vlug, M.A., Schipper, G., Krikor, H.G.T., 1996. Influence of fibre length and concentration on the properties of glass fibre-reinforced polypropylene: Part 3. Strength and strain at failure. Compos. Part A Appl. Sci. Manuf. 27, 1075–1084. https://doi.org/10.1016/1359-835X(96)00066-8.
Tian, J., Cao, Z., Qian, S., Xia, Y., Zhang, J., Kong, Y., Sheng, K., Zhang, Y., Wan, Y., Takahashi, J., 2022. Improving tensile strength and impact toughness of plasticized poly(lactic acid) biocomposites by incorporating nanofibrillated cellulose. Nanotechnol. Rev. 11, 2469–2482. https://doi.org/10.1515/ntrev-2022-0142.
Tian, J., Qian, S., Zhang, Z., Li, Z., Wan, Y., 2023. A facile approach for preparing nanofibrillated cellulose from bleached corn stalk with tailored surface functions. Cellulose 30, 5641–5656. https://doi.org/10.1007/s10570-023-05234-4.
Uppal, N., Pappu, A., Gowri, V.K.S., Thakur, V.K., 2022. Cellulosic fibres-based epoxy composites: from bioresources to a circular economy. Ind. Crops Prod. 182, 114895 https://doi.org/10.1016/j.indcrop.2022.114895.
Wang, J., Geng, C., Luo, F., Liu, Y., Wang, K., Fu, Q., He, B., 2011. Shear induced fiber orientation, fiber breakage and matrix molecular orientation in long glass fiber reinforced polypropylene composites. Mater. Sci. Eng.: A 528, 3169–3176. https://doi.org/10.1016/j.msea.2010.12.081.
Wang, N., Zhang, C., Zhu, W., Weng, Y., 2020. Improving interfacial adhesion of pla/lignin composites by one-step solvent-free modification method. J. Renew. Mater. 8, 1139–1149. https://doi.org/10.32604/jrm.2020.09961.
Yang, J., Ching, Y.C., Chuah, C.H., 2019. Applications of lignocellulosic fibers and lignin in bioplastics: a review. Polym. (Basel) 11, 1–26. https://doi.org/10.3390/polym11050751.
Yang, M., Su, J., Zheng, Y., Fang, C., Lei, W., Li, L., 2023a. Effect of different silane coupling agents on properties of waste corrugated paper fiber/polylactic acid composites. Polym. (Basel) 15, 1–15. https://doi.org/10.3390/polym15173525.
Yang, M., Su, J., Zheng, Y., Fang, C., Lei, W., Li, L., 2023b. Effect of different silane coupling agents on properties of waste corrugated paper fiber/polylactic acid composites. Polym. (Basel) 15, 3525. https://doi.org/10.3390/polym15173525.
Yatigala, N.S., Bajwa, D.S., Bajwa, S.G., 2018. Compatibilization improves physico-mechanical properties of biodegradable biobased polymer composites. Compos Part A Appl. Sci. Manuf. 107, 315–325. https://doi.org/10.1016/j.compositesa.2018.01.011.

Yeo, J.-S., Lee, J.-H., Hwang, S.-H., 2017. Effects of lignin on the volume shrinkage and mechanical properties of a styrene/unsaturated polyester/lignin ternary composite system. Compos B Eng. 130, 167–173. https://doi.org/10.1016/j.compositesb.2017.07.084.

Zhang, M., Lu, J., Li, P., Li, X., Yuan, G., Zuo, Y., 2022. Construction of high-efficiency fixing structure of waterborne paint on silicate-modified poplar surfaces by bridging with silane coupling agents. Prog. Org. Coat. 167, 106846 https://doi.org/10.1016/j.porgcoat.2022.106846.

Zhu, J., Xue, L., Wei, W., Mu, C., Jiang, M., Zhou, Z., 2015. Modification of lignin with silane coupling agent to improve the interface of poly(L-lactic) acid/lignin composites. Bioresources 10, 4315–4325. https://doi.org/10.15376/biores.10.3.4315-4325.